The 4th International Conference
"Advanced Composite Materials Engineering"
COMAT 2012
18- 20 October 2012, Brasov, Romania

PREDICTING GRAIN REFINEMENT BY COLD SEVERE PLASTIC DEFORMATION PROCESSES IN ALLOYS BY USING THE METHOD OF VOLUME AVERAGED DISLOCATION GENERATION

I. Popa [1], V. Geamăn [2]
[1] Universitatea *Transilvania* din Braşov, Romania, ioan.popa@unitbv.ro, geaman.v@unitbv.ro

Abstract: *The grain refinement during severe plastic deformation processes (SPD) is predicted using volume averaged amount of dislocations generated. The model incorporates a new expansion of a model for hardening in the parabolic hardening regime, in which the work hardening depends on the effective dislocation free path related to the presence of non shearable particles and solute-solute nearest neighbour interactions. These two mechanisms give rise to dislocation multiplication in the form of generation of geometrically necessary dislocations and dislocations induced by local bond energies. The model predicts the volume averaged amount of dislocations generated and considers that they distribute to create cell walls and move to existing cell walls/grain boundaries where they increase in the grain boundary misorientation.*
Keywords: *Severe Plastic Deformation (SPD); Equal Channel Angular Pressing (ECAP); Dislocation Mobility; Aluminium Alloys; Grain refinement.*

1. INTRODUCTION

The main purpose of severe plastic deformation (SPD) processes, such as equal channel angular pressing (ECAP, see Fig.1) [28,29,40] and high pressure torsion (HPT, see Fig.2) [6,13,46], is to achieve a refined grain structure. Predicting the grain size attainable through SPD processes is important, because the grain size will determine the strengthening achievable through grain boundary strengthening and because the grain size, especially that related to the stable high angle grain boundaries, has a major influence on superplastic forming properties [4,37]. These SPD processes are mostly conducted under cold deformation conditions, where dynamic recrystallisation is suppressed whilst strain rate dependence is very limited [17]. It is generally thought that FCC metals with grain size 50-100 nm deform predominantly via the slip of lattice dislocations, and for grains larger than 100nm they deform exclusively through this mechanism [47]. Various works have shown that in nanostructured materials (grain size < 50 nm) alternative deformation mechanisms involving deformation twins [20,22,42], and stacking faults (SFs) [8,21] can occur. In some cases these types of defects have even been observed in grains with size up to 100 nm [22], but it is not evident that they make a significant contribution to deformation in these SPD processed materials. Many researchers (see e.g. [36]) consider that the structure evolution during SDP processing broadly follows the classic mechanisms and concepts on structural changes occurring during conventional processes as shown in classic works [1,2,27,30,45]. At the early stage of deformation, a very high dislocation density is introduced, which leads to the formation of an intragranular structure consisting of cells with thick cell walls and low angles of misorientation. As the strain increases, the thickness of the cell walls decreases. These walls evolve into grain boundaries, and ultimately an array of ultra fine grains with high-angle non-equilibrium grain boundaries (GBs) [7,38,39] are formed. (Nonequilibrium grain boundaries may be present where there are non-geometrically necessary dislocations i.e. excess dislocations that do not contribute to the formation of misorientation at a grain boundary.) In broad terms we may term this the classic model for microstructure evolution in highly deformed metals. Xu et al. and Langdon [19,44] noted that the classic model would predict a gradually increasing refinement of the microstructure as a result of the continuous introduction of dislocation during the straining process. However, these researchers considered this to be inconsistent with some experimental observations and an alternative model based on an inter-relationship between the formation of subgrain boundaries and shear deformation during ECAP was proposed [19]. The model incorporates the geometries relevant to repeated ECAP passes (see Fig.1). The original grains become elongated to a band shape subgrain when the billet passes the corner in the first pass. In the second pass, the elongated subgrain is either

further elongated (route C) because the shear plane remains in the same direction or sheared (route A and B_C) because the shear plane is changed to another direction. Especially when route B_C is used, several intersecting slip systems lead to a high density of dislocations and then these dislocations re-arrange and become subsumed in the grain boundary (some researchers consider the latter „ annihilation" of dislocations, as will become clear below we prefer to avoid that term). As a result, for route B_C, a reasonably equiaxed array of grains is formed. Cell wall and grain boundary evolution involves various complex processes [14,17]. Cell wall formation of low angle boundaries by dynamic recovery during the deformation. Low misorientation (1°) boundaries form a 3-d or 2-d cell structure which tends to remain equiaxed during deformation and are sometimes referred to as "incidental dislocation boundaries" [17]. Subgrain size tends to be constant at larger strains, and this is interpreted in terms of a dynamic equilibrium between dislocation generation and annihilation. But also other types of low angle boundaries have been identified. High angle boundaries can form by deformation banding in which grains may split on a coarse scale into several sections which then follow different orientation paths during subsequent deformation, or by increase in misorientation of the persistent boundaries discussed above. However, high angle boundaries may also evolve from low angle boundaries by assimilation of dislocations. Further rigid body rotation during deformation of high angle boundaries, will tend to align them with the rolling plane, thus forming a lamellar microstructure [23].

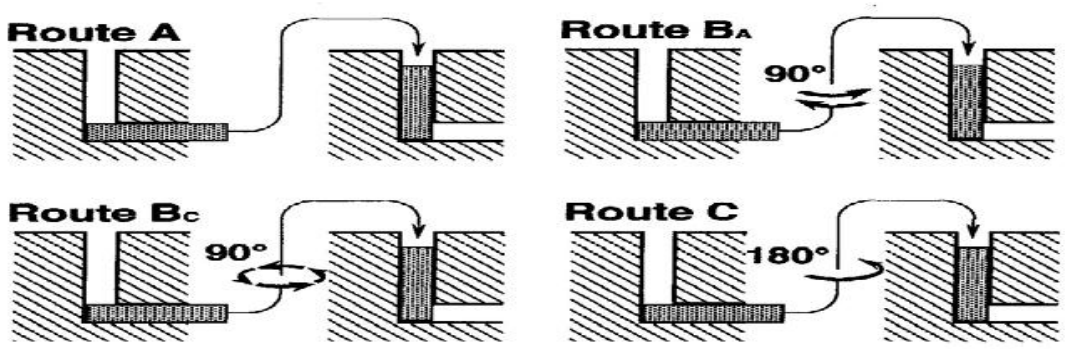

Figure 1: Schematic illustration showing the billet and ECAP die, with the billet rotations during subsequent passes for the 4 basic routes of ECAP. (from [25])

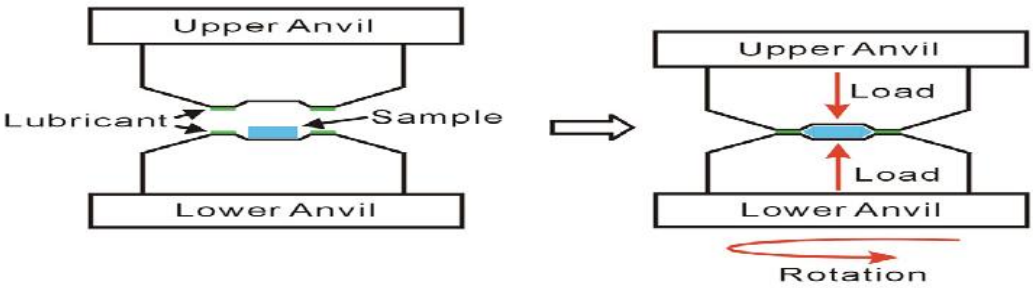

Figure 2: The principle of high pressure torsion (HPT) (from [13])

Grain refinement during SPD is significantly influenced by the presence of non-shearable particles in the alloy, which can produce a factor 2 difference in grain size between alloys with different content of non-shearable particles [24]. Also elements dissolved in the matrix phase have a significant influence on grains refinement, with 3wt%Mg additions to Al causing about a factor 3 reduction in grains size. A model that quantitatively explains these effects has as yet not been available. It has been noted (Beyerlein et.al. [5] and Signorelli et.al. [31]) that prediction of grain size evolution is principle possible in a visco-plastic self-consistent (VPSC) polycrystal model when combined with an (empirical) criterion for the grain subdivision process during ECAP. However, no reports on successful predictions of grain sizes have as yet appeared.The aim of the present work is to derive a model for grain size in the SPD regime incorporating especially the effect of non-shearable particles and dissolved alloying elements. Our new model will employ some of the concepts from the models and papers reviewed above. However, to make the problem tractable, we will use a substantial simplification by treating only averaged dislocation densities as caused by averaged particle spacings and averaged solute contents, effectively reducing a 3D problem to volume averaged properties. This will effectively by-pass much of the details of the cell wall and boundary evolution processes in favour of a model describing a volume averaged behaviour. The model will be tested against microstructure data of several SPD processed Al based alloys. It proved possible to construct a simplified model with good predictive properties in closed form solutions, and

hence we will provide a computationally efficient model. The structure of the present paper is as follows.We will first introduce the materials, processing and experimental techniques applied in the work. Next we will present a model for grain size evolution illustrating several aspects of it with selected results from transmission electron microscopy (TEM) and electron backscatter diffraction (EBSD) work performed. Finally we will present a full description of results and a literature survey on published data for a critical comparison of model predictions with data.

2. EXPERIMENTAL: MATERIALS, PROCESSING AND MICROSTRUCTURE ANALYSIS.

Microstructure development during SPD of 6 alloys was analysed; the compositions of these alloys are given in Table 1. Prior to SPD the Al-7034 and Al-1050 alloys had been extruded into a rod. The Al-2024 alloy was cast, hot rolled to plate and subsequently heat treated to T3 condition. The Al-3Mg-0.2Mn was cast, hot rolled, solution treated and subsequently cold rolled. The other alloys were not thermomechanically processed prior to SPD, they were in as-cast and homogenized condition. The average grain size was 2.1 μm for the 7034 alloy and 45 μm for the 1050 alloy. The grain size for the Al-Zr and Al-Zr-Si-Fe alloys was very large, about 690 μm and 540 μm respectively. The grains in the rolled Al-2024 alloy were pancake shaped with sizes about 100 by 500 μm. The content of second phase particles is very different between these alloys. The 7034 has the highest amount of second phase particles by virtue of the high content of η phase particles present [41]. The amount of second phase particles is intermediate for the 1050 alloy, with the Al-Zr alloy having a very low amount of second phase particles. Five alloys were processed by ECAP and 2 were processed by HPT (see Table 1). ECAP was conducted using a solid die with 9.7 mm diameter channel, with a 90° channel intersection angle (Φ) and a 20° curvature on the outer side of channel intersection (Ψ) (see Fig. 3). Specimens were lubricated with a suspension of MoS_2 in mineral oil ('ASO oil' supplied by Rocol) in order to reduce the friction between the plunger, specimen and the die. A careful alignment of the plunger and upper channel of the die was carried out. A plunger pushing speed of 0.5 mm/s was employed. After one pass of ECAP, another specimen was put in the die to push out the first specimen. Processing of Al-7034 and Al-2024 and selected microstructure analysis results on these alloys was reported before [11,41,43]. All SPD processing was carried out at room temperature, with the exception of ECAP on the Al-7034 alloy which was carried out at 200ºC. Processing by HPT was conducted using disks having diameters of 10 mm and thicknesses of 0.9 mm. All processing by HPT was conducted at room temperature under pressures of 34.0 GPa and with torsional straining between 1 and 5 turns. No lubrication was applied on the sample. In additional tests slippage was found to be negligible. Electron backscattered diffraction (EBSD) was used to characterize the microstructure as well as grain and subgrain boundary misorientation distribution in billets of all ECAP-processed alloys. Samples of 10 mm length used for EBSD analysis were machined from the middle of ECAP-processed billets. For sample preparation, the surface of cross section was first mechanically ground up to 4000-grit SiC paper, then electropolished employing an electrolyte composed of 33 vol% nitric acid and 67 vol% methanol. The electropolishing was carried out with a DC voltage of 20-30 V for 30 seconds. The electrolyte was cooled to and maintained at a temperature of -30°C using liquid nitrogen. The equipment used was a JEOL JSM6500F thermal field emission gun scanning electron microscope (FEG-SEM) equipped with an HKL EBSD detector and HKL Channel 5 software. The SEM accelerating voltage was set to 15 kV. Step size is reported with the results; in most cases it was between 0.1 and 0.5 μm. Orientation imaging microscopy (OIM) maps were obtained from the cross section perpendicular to the longitudinal direction of ECAP-processed billets. Intercept lengths were determined using an automated procedure. For misorientation angle distributions the lowest cut off angle was set at 2°.TEM was conducted on Al-1050 subjected to ECAP and HPT, the Al-Zr alloy subjected to ECAP, and the 2024 alloy subjected to HPT. For TEM disks of 3mm in diameter were punched out from slices cut from the processed billets, ground to about 0.20 mm in thickness and then electropolished using a solution of HNO3 and methanol (1:3 in volume). TEM foils were examined using a JEOL 3010 microscope operating at 300 kV.EBSD analysis of grain size of an HPT processed (5 turns) Al-1Mg-0.3Mn alloy proved unreliable due to very low pattern identification rates, and it was decided to not use EBSD for HPT processed alloys. Instead, to supplement the TEM work on HPT processed samples, the grain size of selected HPT processed samples of an Al-1050 and Al-3Mg-0.3Mn alloys were studied through SEM. For this analysis samples were sectioned, ground and polished, and subsequently etched in Keller's reagent for 3 min. to reveal grain boundaries. SEM was conducted on a JEOL JSM6500F FEG-SEM in secondary electron mode. Grain sizes reported and quoted in this paper were determined through analysis of TEM, EBSD and SEM data. For EBSD analysis of grain sizes on our SPD processed alloys grain boundary intercept lengths, L , were determined using an automated procedure, with lower cut off angle set at 2°. For reliable TEM grain size measurements it needs to be considered that not all grain boundaries in a sample will show a detectable contrast, and also finite sample thickness (causing overlap of grains in the TEM image) needs

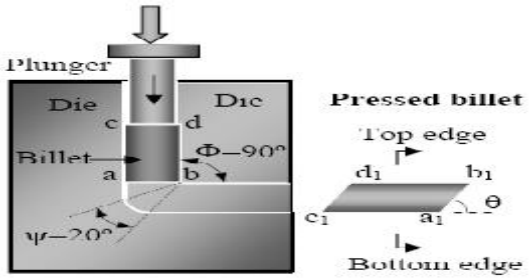

Figure 3: Schematic illustration of the ECAP die.[32]

Table 1: Compositions and grain size for the alloys studied subjected to SPD, with process that the alloys were subjected to.[32]

Alloy	Composition [wt%]							grain size [μm]	SPD	
	Zn	Mg	Cu	Zr	Si	Fe	Mn	before SPD	ECAP	HPT
Al-7034	11.5	2.5	0.9	0.2	-	-	-	2.1	✓	-
Al-1050 A	0.006	0.01	0.009	-	0.12	0.18	0.007	45	✓	-
Al-1050 B	0.006	0	0.008	-	0.14	0.26	0.005	45	-	✓
Al-2024	-	1.4	4.4	-	0.1	0.1	0.4	~200	✓	✓
Al-Zr	<0.01	<0.01	<0.01	0.15	<0.01	<0.01	-	690	✓	-
Al-Zr-Si-Fe	0.01	<0.01	<0.01	0.16	0.17	0.19	-	540	✓	-
Al-3Mg-0.2Mn	0.003	2.95	-	-	0.15	0.20	0.24	30×100	-	✓

to be taken into account. For TEM micrographs obtained for the alloys investigated by us and most TEM micrographs published in the literature, grain size was determined by us by considering only the 20-30% of the micrograph with the lowest beam intensity (i.e. darkest grains) and subsequently eliminating all areas with aspect apparent aspect ratio larger than 2 (because these are likely to be due to overlapping grains). Subsequently intercept lengths were determined on random lines. A correction was made for TEM foil thickness, which is assumed to be 120±50nm.(Note that much of the literature in the field does not seem to consider this correction.) When this procedure produced less than 5 grains, more grains up to at least 5 grains were included. In selected other cases grain size data used, was obtained directly from grain sizes reported in published work (e.g. Ref [33]). We will report accuracies of determinations of average grain size which take into account the uncertainty concerning foil thickness and distribution of sizes. For analysis of SEM micrographs of etched samples, a line intercept method was used. Care was taken to avoid areas where overetching was obscuring grain boundaries. There is a range of ways in which an 'average' grain size can be defined (see e.g. [35]). Although sometimes L has been taken as 'grain size' it is actually an underestimate of most realistic definitions of the grain size, and in this paper we will report the grain size, d, consistently as $d = 1.455\ L$. This is based on $d = V\ 1/3$, V being the average cell volume, with the assumption of a Poisson-Voronoi size/shape distribution. Accuracy of experimental d determinations is typically ±8% (1 standard deviation), rising to ±15% for cases where less than 10 grains can be reliably detected. To elucidate elements of the model, tensile tests were performed on 15 further alloys. The first 9 low Cu Al- Mg-(Cu)-Mn alloys were direct chill (DC) cast, the cast ingots were preheated and homogenised at 540ºC, and subsequently hot rolled down to 5 mm in thickness. After that, the hot rolled and cold rolled to required reduction, and subsequently solution treated at 500ºC. The Al-Cu-Mg and Al-Li-Cu-Mg alloys were produced by conventional casting followed by hot rolling. They were all solution treated at 495ºC. The tensile testing was conducted according to the ASTM-E8M standard. The tensile axis is taken in the longitudinal (L) direction (i.e. the rolling direction). For each condition usually two tests were performed. Tensile tests were performed using an 8800 series Instron machine at a constant strain rate of 0.001 s-1. Selected processing and microstructure data on the Al-Mg-(Cu)-Mn, Al-Cu-Mg and Al-Li-Cu-Mg alloys was reported before [12,18,48].

3. THE MODEL AND SUPPORTING MICROSTRUCTURAL DATA.

3.1 General model structure and main assumptions.

Most available models on grain refinement during SPD follow the strategy of considering the gradual evolution of the microstructure starting from low strains up to the very high strains typical of SPD [3,5,9,17,34]. An important factor in these models is the details of cell wall and subgrain boundary formation. Whilst recognising

the value of those models, especially in elucidating the processes occurring at low and medium strains in 3D, we note that these approaches have not led to a model that is successful in predicting grain sizes of alloys subjected to SPD. In this work will depart from this approach and aim to produce a model that predicts grain sizes in the regime of SPD (effective strains in excess of 3). The model does not include any qualitative predictions on cell and subgrain formation, we just acknowledge that it does occur and is dominant at low to medium strains. We will introduce a substantial simplification in treating only averaged dislocation densities as caused by averaged particle spacings and averaged solute contents, effectively reducing the 3D dislocation movement and cell wall creation case to a volume averaged model. As a consequence the spatial pattern of the grain boundaries has no direct relation to the spatial arrangement of particles and the original orientation of the crystal lattice. We will consider SPD processing routes that lead to grain structures that are close to being equiaxed. Within the model we view a dislocation as being the border of a surface where slip has occurred. It is the cumulative effect of this deformation on a range of slipped surfaces that determines changes in the CW/GB misorientation angle. When a dislocation is assimilated in a CW/GB it may appear „annihilated" in the sense that it can not be discerned in TEM, but in the sense of being the border of a 2D surface where slip has occurred it has not disappeared: it is present in the grain boundary at the intersection of the slipped surface and the grain boundary. (These views are in many ways comparable and compatible to the more elaborate treatments by Estrin, Toth and co-workers [9,34] which incorporates low angle grain boundaries/cell walls of finite thickness and a finite volume density of dislocations. In terms of the concepts these latter works, we are here considering an infinitely thin grain boundary, and an area density of dislocations, and we expand that treatment by extending it to higher angle grain boundaries.). The grain size can be predicted well by considering the total amount of dislocations formed in the straining process, without regard to the detailed geometry and mechanisms of cell wall formation. To simplify terminology we will term any feature that is either a cell wall, low angle grain boundary (LAGB) or high angle grain boundary (HAGB) a „CW/GB" (a cell wall and/or grain boundary). The derivation of the model is described in two parts: dislocation generation formation and evolution of cell walls. The grain size development as a function of the accumulated strain determined in this work and other works [10,15,26] of Al alloys between 99.5 and 99.99wt% purity, and low purity (97wt%) Al (Total equivalent strain during ECAP is determined using the equation described by Iwahashi et.al. [16] and the equivalent strain is determined using the approximation for large strains recommended by Zhilyaev and Langdon [46].). At strains 1 to 3 the CW/GB size is very different between the different alloys.

4. RESULTS AND ANALYSIS: GRAIN SIZE DURING SPD

We have tested the present model for grain size evolution by comparison of its predictions to a range of data on grain size of SPD Al alloys. New data was obtained by performing ECAP on Al-1050, Al-Zr and Al-Zr-Si-Fe alloys and HPT on Al-2024 and Al-3Mg-0.2Mn, size data for a range of other commercial and experimental alloys was obtained from [11,24,33]. The database contains a total of 21 alloys, in a total of 37 alloy-processing combinations, with strains ranging from 1 to 17 and with resulting grain sizes between 2 μm and 50 nm.

5. DISCUSSION

As grain size gets progressively refined, the dislocations created due to the presence of non shearable particles will start to arrive at grain boundaries in ever greater numbers. These dislocations are geometrically necessary in the sense that they are required to create deformation at the non-shearable particle, but they are in general not geometrically necessary in terms of the misorientation angle of the grain boundary. Thus a part of these dislocations will not contribute to misorientation of the grain boundary, and a constellation sometimes described as non equilibrium boundary will result. Thus nonequilibrium boundaries, often observed in SPD metals, are a natural consequence of SPD in the present model. [32]

6. SUMMARY

The work hardening behaviours at strains up to 0.05 and the grain refinement during SPD up to a strain of 16 at room temperature of a wide range of alloys was investigated. A model was presented for the grain refinement and the model for hardening in the parabolic regime was expanded. The work hardening analysis showed: It is confirmed that the work hardening factor depends on the dislocation free path related to the presence of non shearable particles. These particles give rise to dislocation multiplication in the form of generation of geometrically necessary dislocations. [32]

ACKNOWLEDGMENTS

This paper is supported by the Sectoral Operational Programme Human Resources Development (SOP HRD), financed from the European Social Fund and by the Romanian Government under the contract number POSDRU/107/1.5/S/76945.

REFERENCES

[1] Argon, A.S., Haasen, P., Acta. Metall. Mater., 1993, 41:3289.
[2]Ashby, M.F,. In: Kelly, K., Nicholson, R.B., editors. *Strengthening Methods in Crystals*, Elsevier, Amsterdam, The Netherlands, 1971., p.137.
[3] Baik, S.C., et. al., Mater. Sci. Eng., A, 2003, 351:86.
[4] Baretzky, B., et.al., Rev. Adv. Mater. Sci., 2005, 9:45.
[5] Beyerlein, I.J., Lebensohn, R.A., Tome, C.N., Mater. Sci. Eng., A, 2003, 345:122.
[6] Bridgman, P.W., *Studies in large plastic flow and fracture*, McGraw-Hill, 1952, New York, USA.
[7] Chang, C.P., Sun, P.L., Kao, P.W., Acta Mater., 2000, 48:3377
[8] Chen, M.W., et.al., Science, 2003, 300:1275.
[9] Estrin, Y., et. al., Acta Mater., 1998, 46:5509.
[10]Field, D.P., Weiland, H., In: Schwartz, A.J., Kumar, M., Adams, B.L., editors. *Electron Backscatter Diffraction in Materials Science*, Kluwer Acad., New York, 2000, p. 199.
[11] Gao, N., et. al., Mater. Sci. Eng., A, 2005, 410-411:303.
[12] Gao, N., et. al., Mater. Sci. Tech., 2005, 21:1010.
[13] Horita, Z., Langdon, T.G., Mater. Sci. Eng. A, 2005, 410-411:422.
[14] Hughes, D.A., Mater. Sci. Eng., A, 2001, 319:46.
[15] Iwahashi, Y., et.al., Acta Mater., 1998, 46:3317.
[16] Iwahashi Y, et. al., Scripta Mater., 1996, 35:143.
[17] Jazaeri, H., Humphreys, F.J., Acta Mater., 2004, 52:3239 .
[18] Kamp, N., et. al., Int. J. Fatigue, 2007, 29:869.
[19] Langdon, T.G., Mater. Sci. Eng. A, 2007, 462:3.
[20] Liao, X.Z., et.al., Appl. Phys. Lett., 2004, 84:592.
[21] Liu, M.P., et. al., Mater. Sci. Eng., A, 2008, 483-484:59.
[22] Liu, M.P., et. al., Mater. Sci. Eng., A, 2009, 503:122.
[23] Liu, Q., et. al., Acta Mater., 2002, 50:3789.
[24] Munoz Morris, M.A., Gutierrez-Urrutia, I., Morris, D.G., Mater. Sci. Eng., A, 2008, 493:141.
[25] Nakashima K., et. al., Mater. Sci. Eng., 2000, A281:82.
[26] Reihanian, M., et. al., Mater Char., 2008, 59:1312.
[27] Rollett, A.D., Kocks, U.F., Solid State Phenomena, 1994, 35-36:1.
[28] Segal V.M, et. al., Russian Metall, 1981, 1:99.
[29] Segal V.M., Mater. Sci. Eng. A, 1995, 97:57.
[30] Sevillano, J.G., Aernoudt, E., Mater. Sci. Eng., A, 1987, 86:35.
[31] Signorelli, J.W., et. al., Scripta Mater., 2006, 55:1099.
[32] Starink, M. J., et.al., *Predicting grain refinement by cold severe plastic deformation in alloys using volume averaged dislocation generation,* Acta Mater., 2009, SO171BJ, UK.
[33] Stolyarov, V.V., et. al., Mater. Sci. Eng., A, 2003, 357:159.
[34] Toth, L., Molinari, A., Estrin, Y. J., Eng. Mater. Tech., 2002, 124:71.
[35] Underwood, E., Quantitative Stereology, Addison-Wesley, Cambridge Massachusetts, 1970.
[36] Valiev, R.Z., et.al., Acta. Mater., 1996, 44:4705.
[37] Valiev, R.Z., et.al., Scripta Mater. 1997, 37:1945.
[38] Valiev, R.Z., Islamgaliev, R.K., Alexandrov, I.V., Prog. Mater. Sci., 2000, 45:103.
[39] Valiev, R.Z., Nat. Mater., 2004, 3:511.
[40] Valiev R.Z., Langdon, T.G., Prog. Mater. Sci., 2006, 51:881.
[41] Wang, S.C., et. al., Rev. Adv. Mater. Sci., 2005, 10:249.
[42] Wu, X.L., Ma, E., Zhu, Y.T.J., Mater. Sci., 2007, 42:1427.
[43] Xu, C., et. al., Mater. Lett., 2003, 57:3588.
[44] Xu, C., et. al., Mater. Sci. Eng., A, 2005, 398:66.
[45] Zehetbauer, M., Seumer, V., Acta Metall Mater., 1993, 41:577.
[46] Zhilyaev, A.P., Langdon, T.G., Prog. Mater. Sci., 2008, 53:893.
[47] Zhu, Y.T., Langdon, T.G., Mater. Sci. Eng. A, 2005, 409:242.
[48] Zhu, Z., Starink, M.J., Mater. Sci. Eng., A, 2008, 489:138.